Supplementary Information

Spin-crossover in iron(III) complex showing a broad thermal hysteresis

Cyril Rajnák [a], Romana Mičová [a], Ján Moncoľ [b], Ľubor Dlháň [b], Christoph Krüger [c], Franz Renz [c], Roman Boča [a]

[a] *Department of Chemistry, Faculty of Natural Sciences, University of SS Cyril and Methodius, 91701 Trnava, Slovakia,*
[b] *Institute of Inorganic Chemistry, FCHPT, Slovak University of Technology 81237 Bratislava, Slovakia*
[c] *Institute of Inorganic Chemistry, Leibniz University Hannover, 30167 Hannover, Germany*

Abbreviations

[Fe(^{3,5}Cl-L)Cl], (**1a**), $C_{19}H_{17}FeN_3O_2Cl_5$
[Fe(^{3,5}Cl-L)(N_3)] (**1b**), $C_{19}H_{17}FeN_6O_2Cl_4$
[Fe(^{3,5}Cl-L)(NCS)], (**1c**), $C_{20}H_{17}FeN_4O_2Cl_4S$
[Fe(^{3,5}Cl-L)(NCSe)], (**1d**), $C_{20}H_{17}FeN_4O_2Cl_4Se$
[Fe(^{3,5}Br-L)Cl], (**2a**), $C_{19}H_{17}FeN_3O_2ClBr_4$
[Fe(^{3,5}Br-L)(N_3)], (**2b**), $C_{19}H_{17}FeN_6O_2Br_4$
[Fe(^{3,5}Br-L)(NCS)], (**2c**), $C_{20}H_{17}FeN_4O_2Br_4S$
[Fe(^{3,5}Br-L)(NCSe)], (**2d**), $C_{20}H_{17}FeN_4O_2Br_4Se$

Synthesis of [Fe(^{3,5}X-L)(Cl)] type precursors

N-(2-aminoethyl)-1,3-propanediamine (10 mmol) and 3,5-dichlorosalicylaldehyde and/or 3,5-dibromosalicylaldehyde (20 mmol) were dissolved in 120 cm^3 of methanol. The solution was stirred and heated under reflux for 15 min, $FeCl_3 \cdot 6H_2O$ (10 mmol) in 25 cm^3 methanol was added and further stirred and heated under reflux for 1 h. After cooling to -18 Celsius for 24 h, black microcrystalline product was filtered off and dried at room temperature. The reaction scheme is shown in Fig. S1.

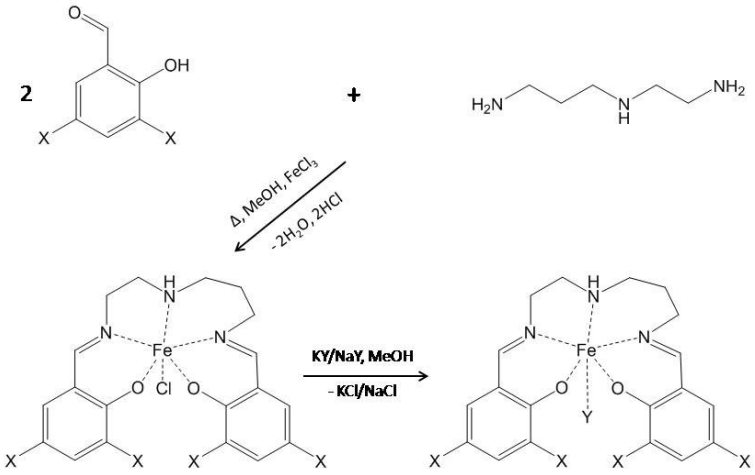

Fig. S1. Sketch of the pentadentate ligands 3,5-Cl-*salpet*, 3,5-Br-*salpet* (X = Cl or Br) and their complexes [Fe(^{3,5}X-L)(Y)] (Y = N_3^-, NCS^- and $NCSe^-$).

Data for [Fe(^{3,5}Cl-L)Cl], (**1a**). $C_{19}H_{17}FeN_3O_2Cl_5$ yield 4.2 g (76 %), (M = 552.48 g mol^{-1}) Calculated: C, 41.3 %; H, 3.10 %; N, 7.6 %. Found: C, 41.0 %; H, 3.05 %; N, 7.5 %; ESI-MS: [Fe(^{3,5}Cl-L)]$^+$: Calculated = 516.94 g mol^{-1}; Found: 516.90 g mol^{-1}. IR: ν(N-H) = 3260 cm^{-1}, ν(C-H) = 2901 cm^{-1}, ν(C=N) = 1638, 1610 cm^{-1}.

Data for [Fe(^{3,5}Br-L)Cl], (**2a**). $C_{19}H_{17}FeN_3O_2ClBr_4$ yield 3.72 g (51 %), (M = 730.28 g mol^{-1}) Calculated: C, 31.3 %; H, 2.35 %; N, 5.8 %. Found: C, 31.4 %; H, 2.44 %; N, 5.6 %. ESI-MS: [Fe(^{3,5}Br-L)]$^+$: Calculated = 694.74 g mol^{-1}; Found: 694.68 g mol^{-1}. IR: ν(N-H) = 3050 cm^{-1}, ν(C=N) = 1633, 1609 cm^{-1}.

Synthesis of [Fe(^{3,5}X-L)(Y)] complexes

Pseudohalide salt KY or NaN_3 (0.42 mmol) was dissolved in 30 cm^3 methanol and added to a solution of [Fe(^{3,5}X-L)Cl] (0.4 mmol) in 100 cm^3 methanol. The mixture was stirred in an ultrasonic bath for 5 min. and filtered by a paper filter afterwards.

Data for [Fe(^{3,5}Cl-L)(N_3)] (**1b**). $C_{19}H_{17}FeN_6O_2Cl_4$ yield 0.19 g (83 %), (M = 559.03 g mol^{-1}) Calculated: C, 40.8 %; H, 3.07 %; N, 15.0 %. Found: C, 40.8 %; H, 2.96 %; N, 14.9 %. IR (Tr): ν(N-H) = 3244 cm^{-1}, ν(C-H) = 2903 cm^{-1}, ν(N_3) = 2085 cm^{-1}, ν(C=N) = 1632, 1610 cm^{-1}.

Data for [Fe(^{3,5}Cl-L)(NCS)], (**1c**). $C_{20}H_{17}FeN_4O_2Cl_4S$ yield 0.2 g (85 %), (M = 575.11 g mol^{-1}) Calculated: C, 41.8 %; H, 2.98 %; N, 9.7 %. Found: C, 41.5 %; H, 2.91 %; N, 9.6 %. IR (Tr): ν(N-H) = 3265 cm^{-1}, ν(C-H) = 2902 cm^{-1}, ν(NCS) = 2036 cm^{-1}, ν(C=N) = 1639,1618 cm^{-1}.

Data for [Fe(^{3,5}Cl-L)(NCSe)], (**1d**). $C_{20}H_{17}FeN_4O_2Cl_4Se$ yield 0.2 g (82 %), (M = 621.99 g mol^{-1}) Calculated: C, 38.6 %; H, 2.75 %; N, 9.0 %. Found: C, 38.7 %; H, 2.64; N, 9.0 %. IR (Tr): ν(N-H) = 3266 cm^{-1}, ν(C-H) = 2904 cm^{-1}, ν(NCSe) = 2037 cm^{-1}, ν(C=N) = 1640, 1619 cm^{-1}. The single crystals were obtained by slow evaporation of the mother liquor at room temperature after couple of days.

Data for [Fe(^{3,5}Br-L)(N_3)], (**2b**). $C_{19}H_{17}FeN_6O_2Br_4$ yield 0.13 g (44 %), (M = 736.85 g mol^{-1}) Calculated: C, 31.0 %; H, 2.33 %; N, 11.4 %. Found: C, 30.9 %; H, 2.41 %; N, 11.4 %. IR (Tr): ν(N-H) = 3241 cm^{-1}, ν(C-H) = 2928 cm^{-1}, ν(N_3) = 2084 cm^{-1}, ν(C=N) = 1631, 1609 cm^{-1}.

Data for [Fe(^{3,5}Br-L)(NCS)], (**2c**). $C_{20}H_{17}FeN_4O_2Br_4S$ yield 0.13 g (42 %), (M = 752.91 g mol^{-1}) Calculated: C, 31.9 %; H, 2.28 %; N, 7.4 %. Found: C, 31.5 %; H, 2.23 %; N, 7.0 %. IR (Tr): ν(N-H) = 3243 cm^{-1}, ν(C-H) = 2926 cm^{-1}, ν(NCS) = 2036 cm^{-1}, ν(C=N) = 1637, 1616 cm^{-1}.

Data for [Fe(^{3,5}Br-L)(NCSe)], (**2d**). $C_{20}H_{17}FeN_4O_2Br_4Se$ yield 0.13 g (40 %), (M = 799.80 g mol^{-1}) Calculated: C, 30.0 %; H, 2.14 %; N, 7.0 %. Found: C, 30.3 %; H, 2.18 %; N, 6.5 %. IR (Tr): ν(N-H) = 3246 cm^{-1}, ν(C-H) = 2909 cm^{-1}, ν(NCSe) = 2038 cm^{-1}, ν(C=N) = 1637, 1616 cm^{-1}.

Table S1. Crystallographic data for compounds **1a** and **1d.**

	1a	**1d**	**1d'**
Chemical formula	$C_{19}H_{17}Cl_5FeN_3O_2$	$C_{20}H_{17}Cl_4FeN_4O_2Se$	$C_{20}H_{17}Cl_4FeN_4O_2Se$
M_r	552.45	621.99	621.99
Crystal system	Monoclinic	Monoclinic	Monoclinic
Space group	$P2_1/c$	$P2_1/n$	$P2_1/n$
T / K	293(1)	**100(1)**	**200(1)**
a / Å	9.3482(3)	8.3908(2)	8.4121(3)
b / Å	9.4215(2)	22.2708(6)	23.8983(6)
c / Å	25.8019(8)	12.6870(4)	12.1560(4)
α / °	90	90	90
β / °	94.432(2)	103.222(2)	106.571(3)
γ / °	90	90	90
V / Å^3	2265.68(11)	2307.97(11)	2344.02(13)
Z	4	4	4
λ / Å	1.54186	1.54186	1.54186
Abs. correction	Multi-scan, LANA	Multi-scan, LANA	Multi-scan, LANA
μ / mm^{-1}	10.954	11.537	11.360
Crystal size / mm	0.18 × 0.14 × 0.12	0.12 × 0.05 × 0.04	0.25 × 0.05 × 0.04
ρ_{calc} / g.cm^{-3}	1.620	1.790	1.762
S	1.037	1.056	1.105
R_1 [I> 2σ(I)]	0.0414	0.0670	0.0906
wR_2 [all data]	0.1053	0.1880	0.2605
CCDC no.	2035917	2035918	2035919

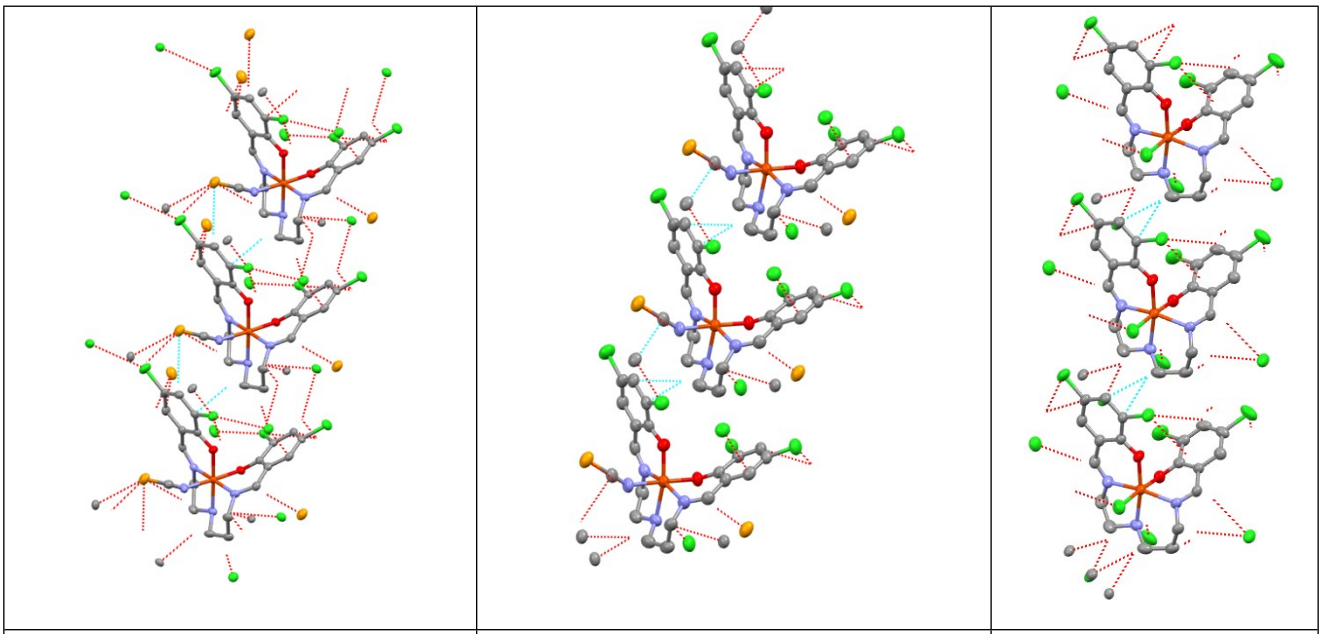

1d, LS | **1d'**, HS | **1a**, HS

Fig. S2. Comparison of intermolecular contacts.

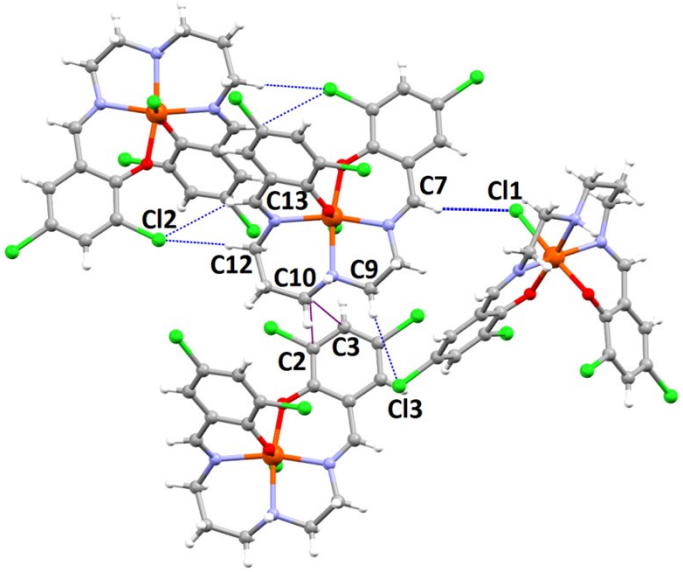

Fig. S3. The hydrogen bonding interactions in crystal structure of **1a**.

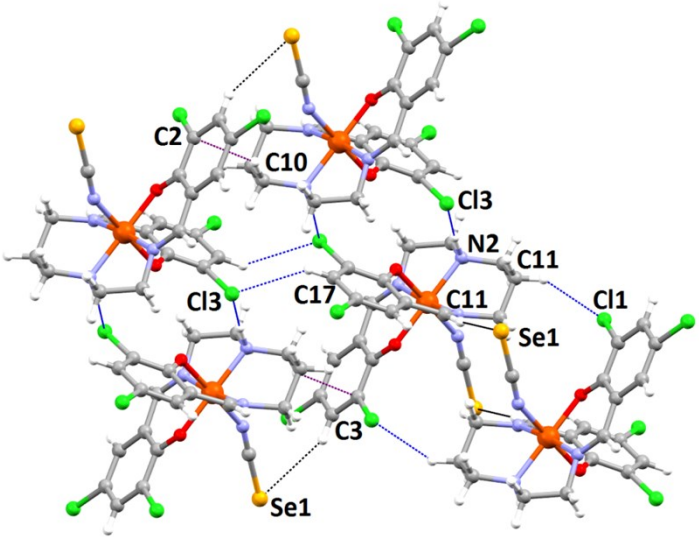

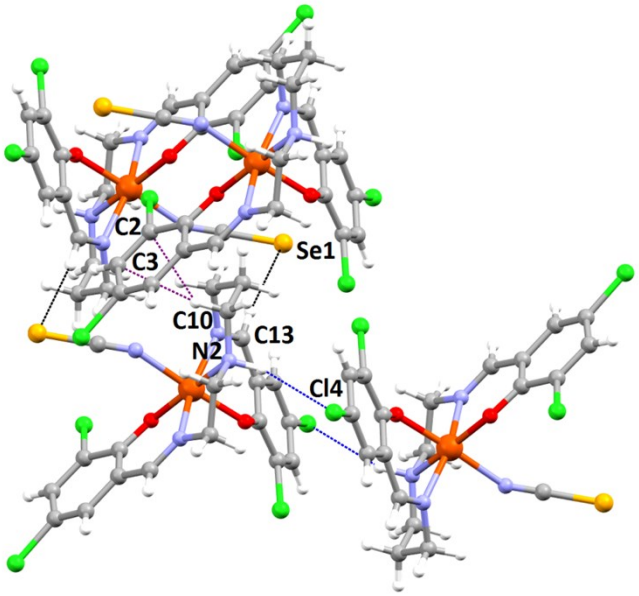

Fig. S4. The hydrogen bonding interactions in crystal structure of **LS 1d** at 100 K (top) and **HS 1d'** at 200 K (bottom).

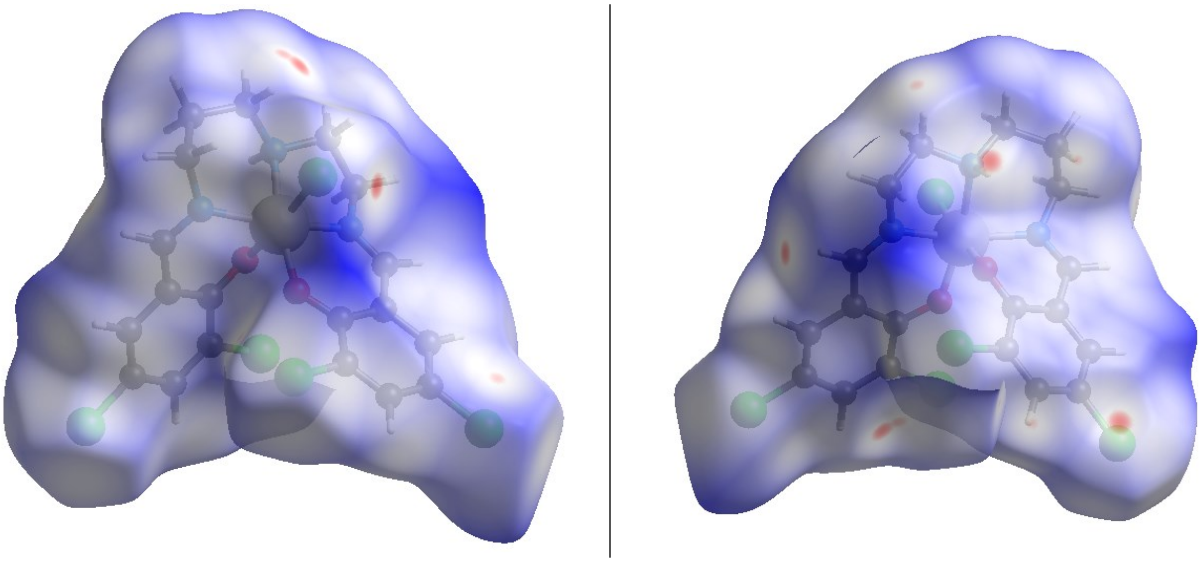

Fig. S5. View of the three-dimensional Hirshfeld surface of **1a** plotted over d_{norm} in the range -0.0780 to 1.8739 a.u.

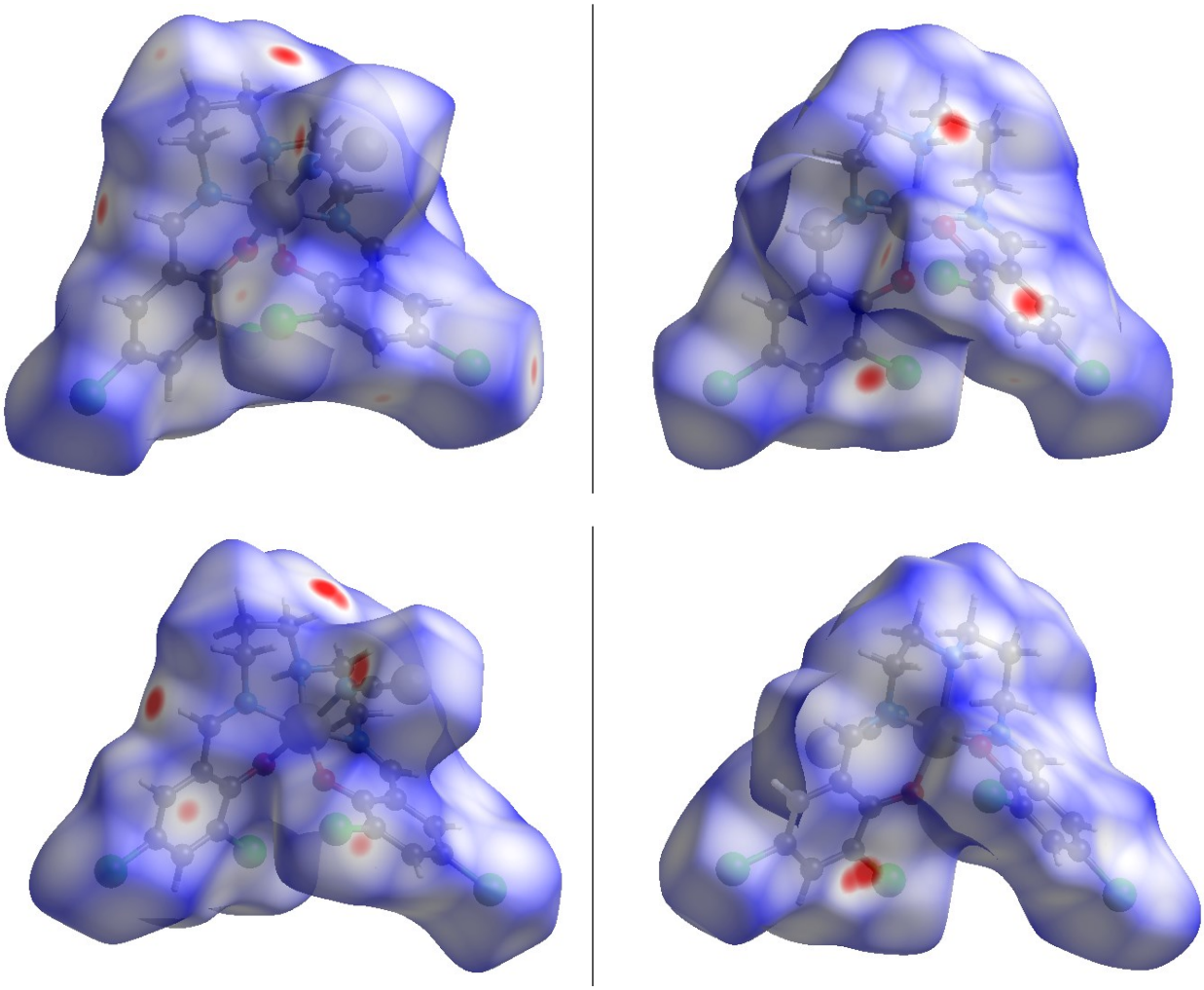

Fig. S6. View of the three-dimensional Hirshfeld surface of **1d** plotted over d_{norm} in the range -0.0780 to 1.8739 a.u. LS at 100 K (top) and HS at 200 K (bottom).

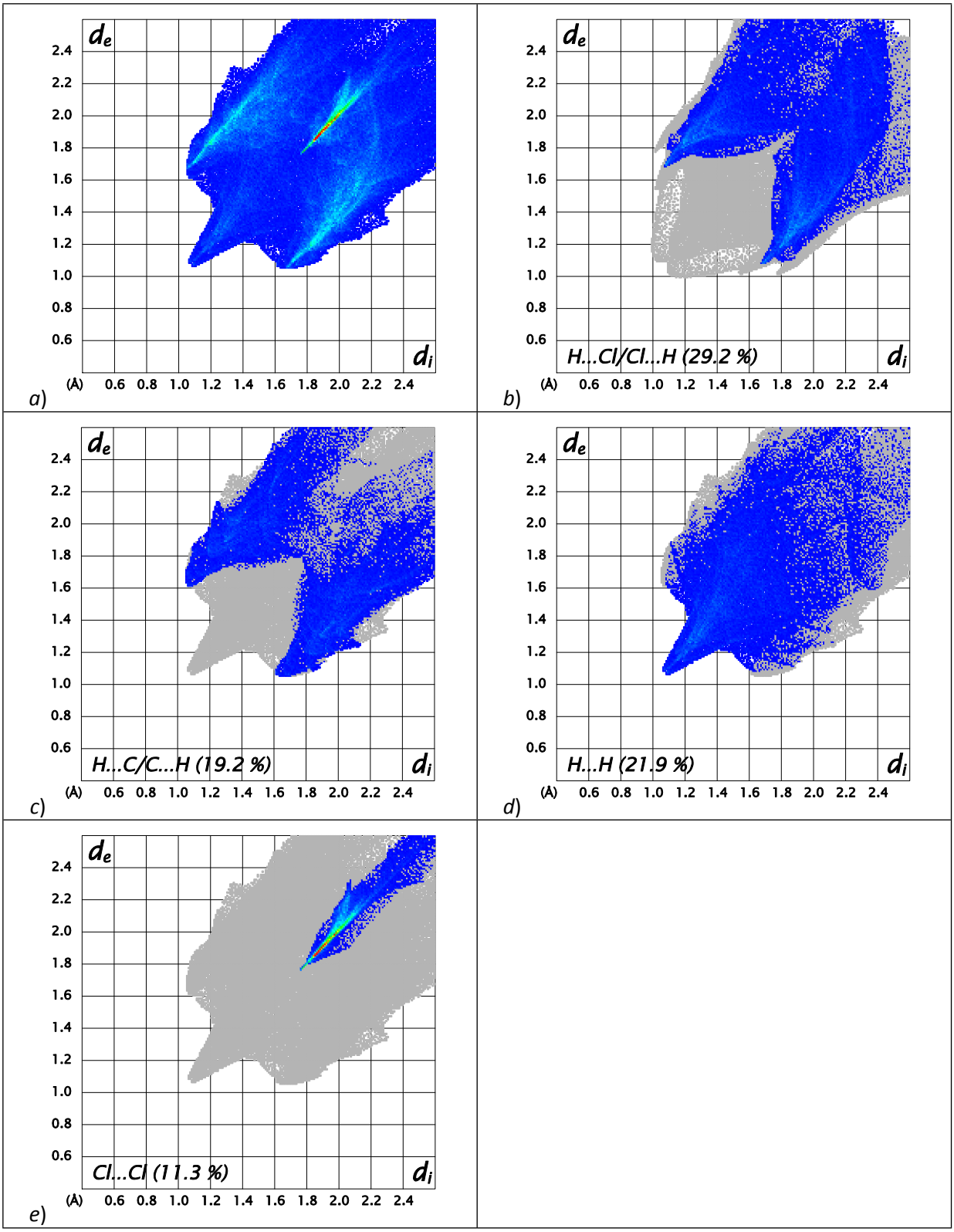

Fig. S7. The full two-dimensional fingerprint plots of **1a**, showing (*a*) all interactions, (b) H···C/Cl···H, (c) H···C/C···H, (*d*) H···H, and (*e*) Cl···Cl interactions. The d_i and d_e values are the closest internal and external distances from given on the Hirshfeld surface contacts.

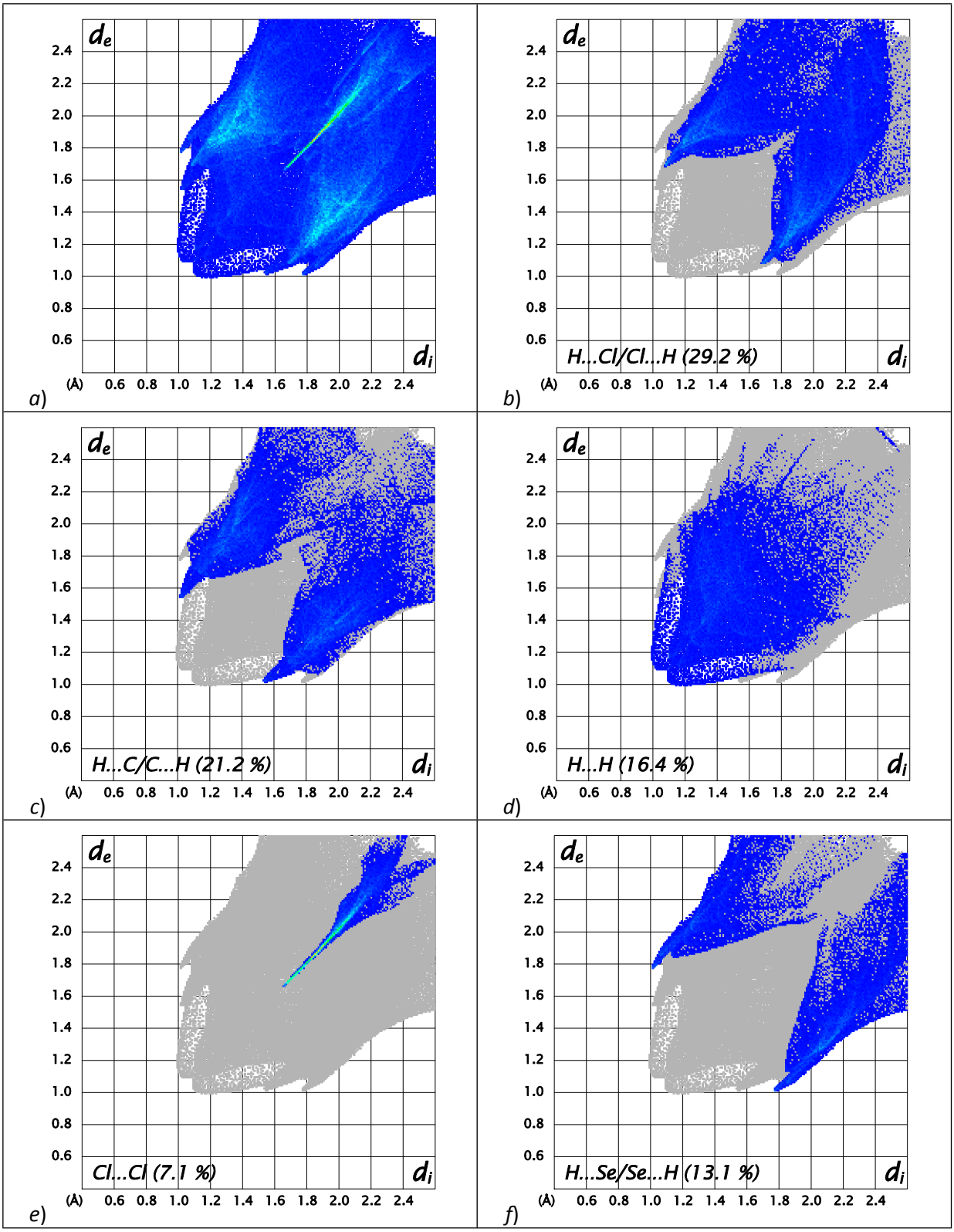

Fig. S8. The full two-dimensional fingerprint plots of **1d** at 100 K, showing (*a*) all interactions, (b) H···C/Cl···H 29.2%, (c) H···C/C···H 21.2%, (*d*) H···H 16.4%, (*e*) Cl···Cl 7.1%, and (*f*) H···Se/Se···H 13.1% interactions. The d_i and d_e values are the closest internal and external distances from given on the Hirshfeld surface contacts.

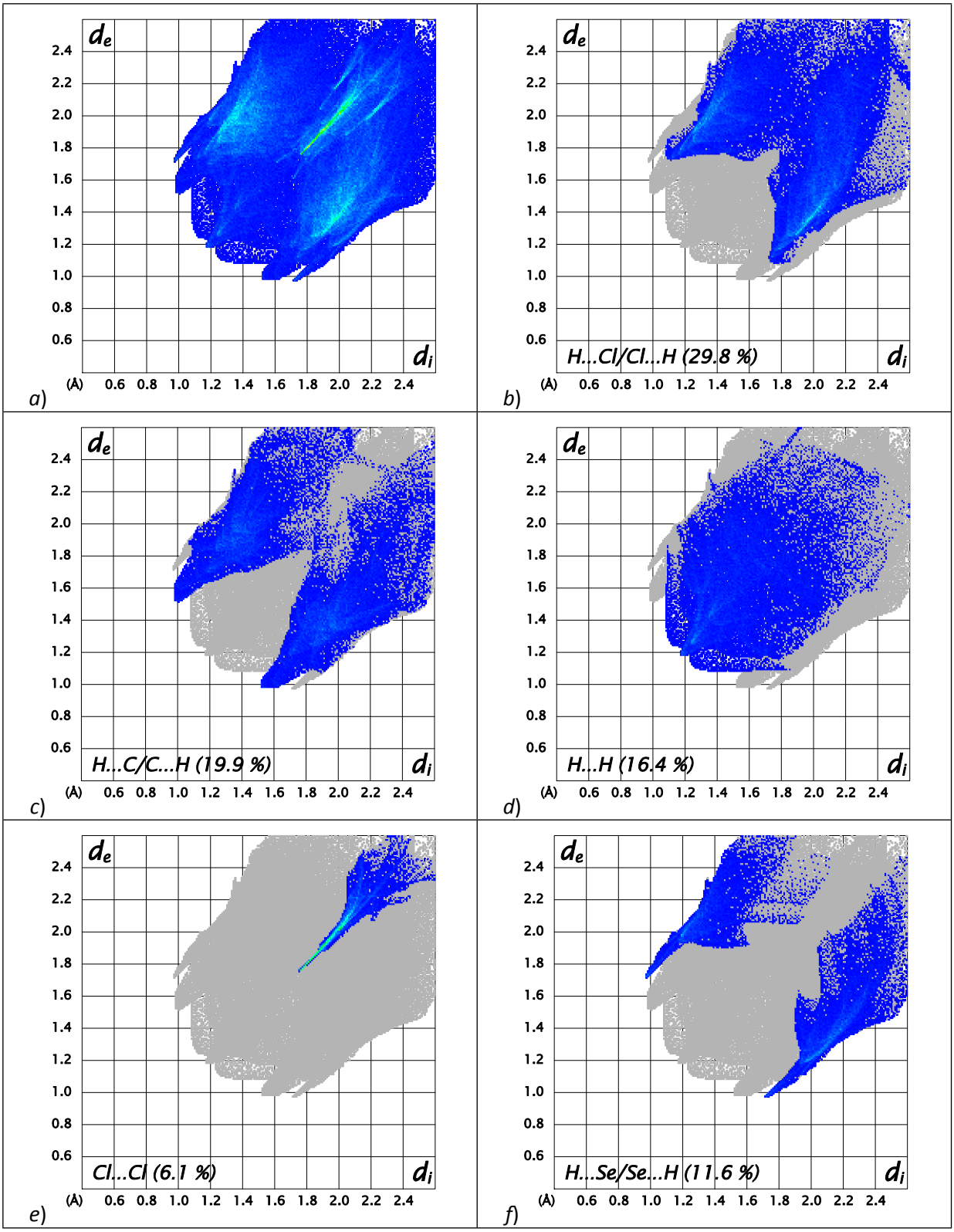

Fig. S9. The full two-dimensional fingerprint plots of **1d'** at 200 K, showing (*a*) all interactions, (b) H···Cl/Cl···H 29.8%, (c) H···C/C···H 19.9%, (*d*) H···H 16.4%, (*e*) Cl···Cl 6.1%, and (*f*) H···Se/Se···H 11.6% interactions. The d_i and d_e values are the closest internal and external distances from given on the Hirshfeld surface contacts.

Explanations to Hirshfeld surfaces and fingerprint plots
[M. A. Spackman and D. Jayatilaka, *CrystEngComm*, 2009, **11**, 19]

Function	Symbol and definition	Mapping range
distance from a point on the surface to the nearest nucleus *outside* the surface	d_e	red (short distances) through green to blue (long distances)
distance from a point on the surface to the nearest nucleus *inside* the surface	d_i	red (short distances) through green to blue (long distances)
shape index, S, a measure of "*which*" shape, defined in terms of principal curvatures κ_1 and κ_2	$S = \frac{2}{\pi}\arctan\left(\frac{\kappa_1 + \kappa_2}{\kappa_1 - \kappa_2}\right)$	−1.0 (concave) through 0.0 (minimal surface) to +1.0 (convex)
curvedness, C, a measure of "*how much*" shape,, defined in terms of principal curvatures κ_1 and κ_2	$C = \frac{2}{\pi}\ln\sqrt{\kappa_1^2 + \kappa_2^2/2}$	−4.0 (flat) through 0.0 (unit sphere) to +0.4 (singular)
normalized contact distance, defined in terms of d_e, d_i and the vdW radii of the atoms	$d_{norm} = \frac{d_i - r_i^{vdW}}{r_i^{vdW}} + \frac{d_e - r_e^{vdW}}{r_e^{vdW}}$	red (distances shorter than sum of vdW radii) through white to blue (distances longer than sum of vdW radii)

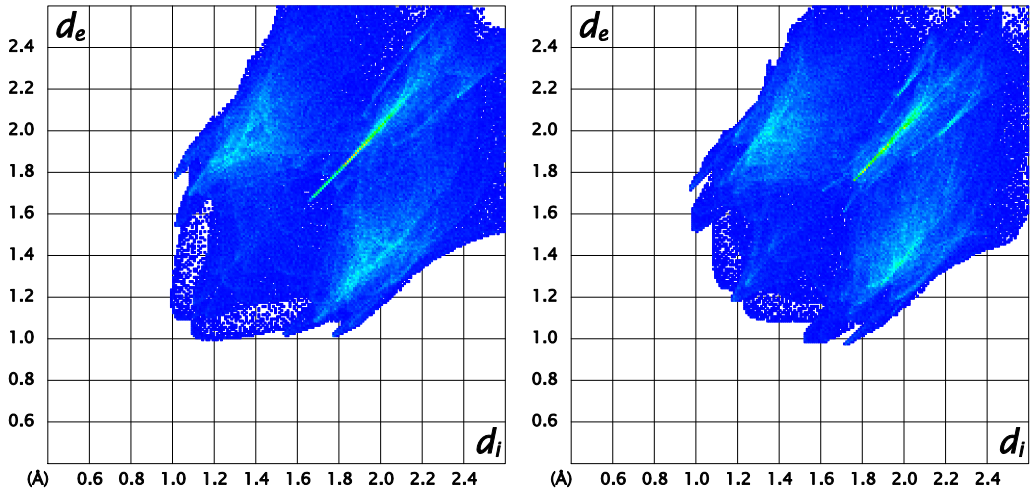

Fig. S10. Comparison of the fingerprint plots of all interactions for **1d** 100 K (left) and **1d'** 200 K (right) systems.

- There is a shift of the overall area to higher values on heating.
- Light area with increased histogram (green to red) is moved to higher values.
- Percentage of the critical contacts H-C/C-H, Cl…Cl and H-Se/Se-H decreases on heating:

Contacts [%]	**100 K**	**200 K**
H-Cl/Cl-H	29.2	29.8
H-C/C-H	21.2	19.9
H…H	16.4	16.4
Cl…Cl	7.1	6.1
H-Se/Se-H	13.1	11.6
other	13	16.2
sum [%]	87	83.8

Magnetic data

SQUID magnetometer (Quantum Design, MPMS-XL7) was used in the magnetic data taking: temperature dependence of the magnetic susceptibility, and field dependence of the magnetization; RSO mode of the data acquisition at B_{DC} = 0.1 T was used. A correction to the underlying diamagnetism was applied to raw magnetic data. They were transformed to the temperature dependence of the effective magnetic moment, and the field dependence of the magnetization per formula unit.

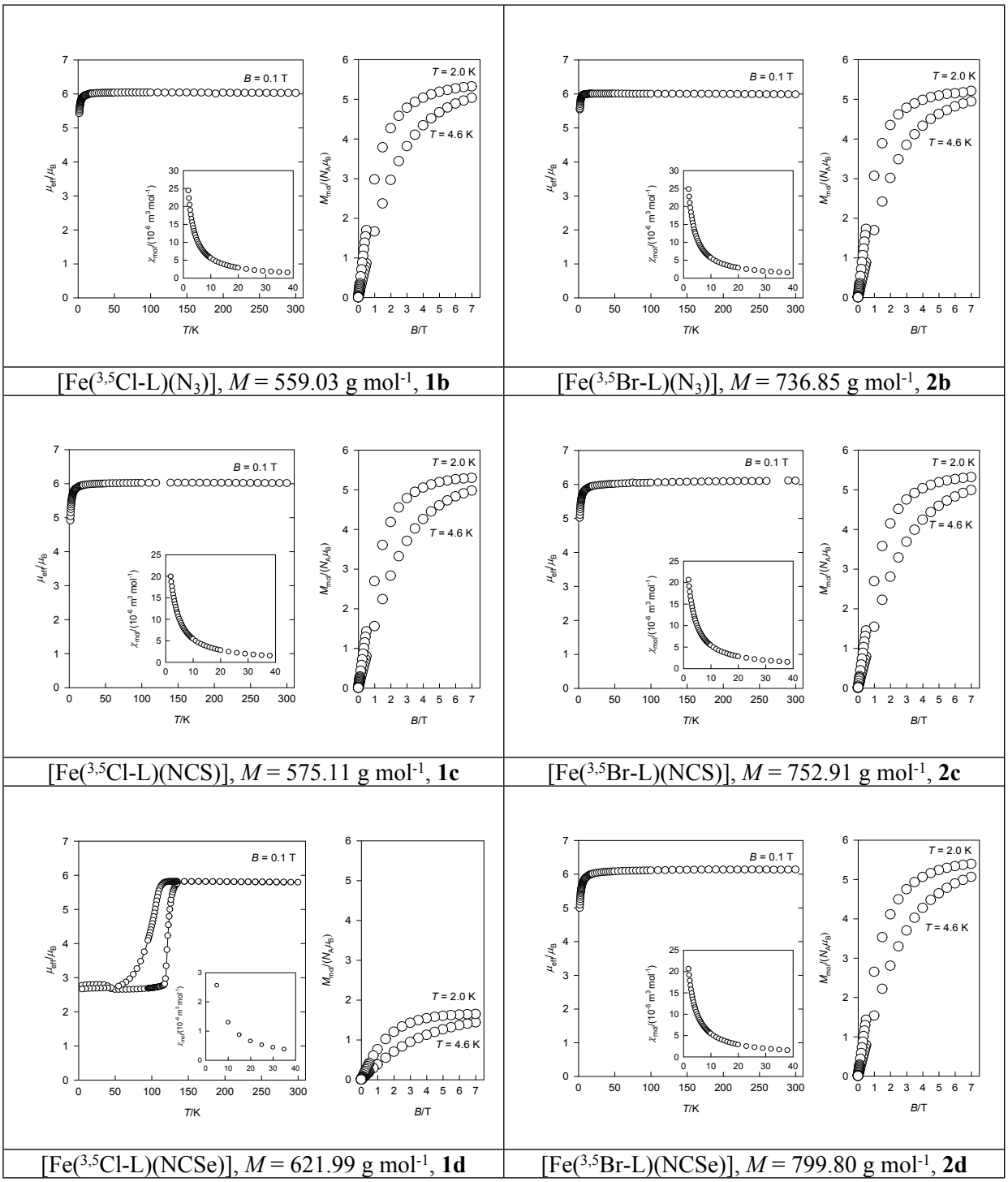

[Fe(^{3,5}Cl-L)(N_3)], M = 559.03 g mol^{-1}, **1b**

[Fe(^{3,5}Br-L)(N_3)], M = 736.85 g mol^{-1}, **2b**

[Fe(^{3,5}Cl-L)(NCS)], M = 575.11 g mol^{-1}, **1c**

[Fe(^{3,5}Br-L)(NCS)], M = 752.91 g mol^{-1}, **2c**

[Fe(^{3,5}Cl-L)(NCSe)], M = 621.99 g mol^{-1}, **1d**

[Fe(^{3,5}Br-L)(NCSe)], M = 799.80 g mol^{-1}, **2d**

Fig. S11. Magnetic functions for the high spin complexes of [Fe(^{3,5}X-L)(Y)] type.

Temperature dependence of the magnetic susceptibility has been a subject of the fitting to an Ising/like model of spin crossover with vibrations. In fitting the magnetic data some assumptions have been made. (i) The low-spin state of Fe(III) is well described by the Curie-Weiss law enlarged by the temperature-independent (van Vleck) term. The free parameters are the g_L-factor, the Weiss constant Θ_L, and α_L. (ii) The same holds true for the high-spin state, however one can safely fix $g_H = 2.0$ and omit Θ_H and α_H. (iii) There is nothing like a paramagnetic impurity for the Fe(III) complex (as opposite to a frequent situation for Fe(II) ones). The fourth assumption postulates a model of the spin crossover. This model contains four parameters: (i) the energy difference between LS and HS state Δ_{eff} that is proportional to the enthalpy of the spin transition $\Delta H = R{\cdot}E$; (ii) the solid-state cooperativeness J (not to be confused with the exchange coupling constant); (iii) two averaged vibrational frequencies (in fact the Einstein modes) that enter the vibrational partition function. In such a model the equation

$$\langle\sigma\rangle_T = \frac{F-1}{F+1} \tag{S1}$$

with

$$f = \exp[-(E - kT\ln r_{\mathrm{eff}}^T - 2\Gamma\langle\sigma\rangle_T)/kT] \tag{S2}$$

is to be iterated in order to achieve a selfconsistency. The high-spin mole fraction is related to an fictitious spin *via* $x_H = (1+\langle\sigma\rangle_T)/2$; the entropic factor is

$$r_{\mathrm{eff}}^T = \frac{g_H^{\mathrm{el}}}{g_H^{\mathrm{el}}}\left[\frac{1-\exp(h\bar{\nu}_L/kT)}{1-\exp(h\bar{\nu}_H/kT)}\right]^m \tag{S3}$$

for m = 15 active modes in a hexacoordinate complex, $h\bar{\nu}_H$ and $h\bar{\nu}_L$ – averaged vibration energies. The transition entropy is then $\Delta S = R\,r_{\mathrm{eff}}^T\big|_{x_H=1/2}$. To this end the equilibrium constant is calculated as $K = x_H(1-x_H)$ and this can be used in generating the van't Hoff plot ln$K$ *vs* T^{-1}.

The model can be modified by considering a frozen portion of the HS-fraction (equivalent to the fixed paramagnetic impurity x_{PI}). In such a case the g_{LS} is much closer to the spin-only value, typically g_{LS} = 2.2 – 2.3. The resulting thermodynamic parameters of the spin crossover such as ΔH, ΔS, T_c and Γ are almost the same.

The data fitting has been done using the program MIF&FIT [R. Boča, Program MIF with FIT module. University of SS Cyril and Methodius, Trnava, © 2019].

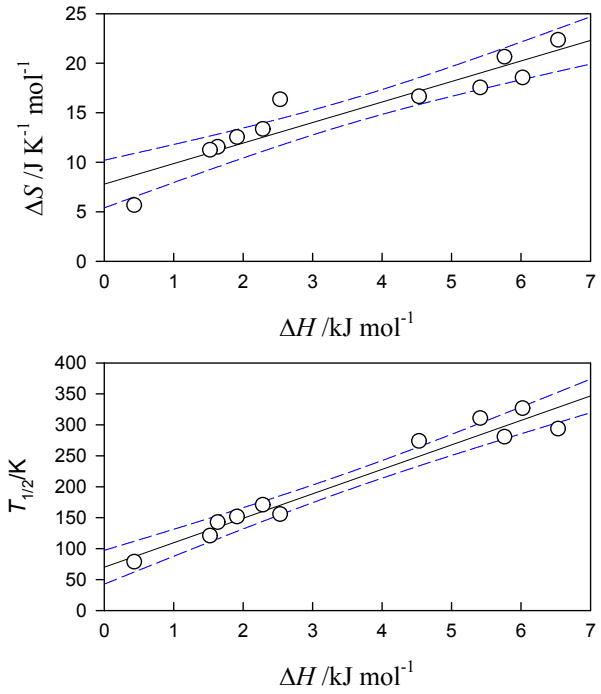

Fig. S12. Correlation of thermodynamic parameters for the spin crossover compounds.

Table S3. Thermodynamic parameters for mutually related Fe(III) spin crossover complexes. [a]

	Compound	$T_{1/2}$ /K	$\Delta T_{1/2}$ /K	ΔH /kJ mol^{-1}	ΔS /J K^{-1} mol^{-1}	(Γ/k_B) /K	Ref.
1	[Fe(^{3}EtO-*saldet*)(NCS)]	84 ↑, 82 ↓ *	2	0.98; 2.07	11.8; 5.0	90	S5
2	[Fe(^{3,5}Cl-*salpet*)(NCSe)], **1d**	123 ↑, 99 ↓	24	2.03	17.6	153	This work
3	[Fe(^{5}Br-*salpet*)(N_3)]·MeOH	142		1.64	11.5	76	S1
4	[Fe(^{5}Cl-*salpet*)(NCS)]	280		5.77	20.6	180	S2
5	[Fe(^{5}Cl-*salpet*)(NCSe)]	293		6.54	22.3	197	S2
6	[Fe(^{5}Br-*salpet*)(NCSe)]	326		6.03	18.5	215	S1
7	[Fe(^{5}Cl-*saldpt*)py]BPh_4	78		0.44	5.61	63	S3
8	[Fe(^{3}MeO-*saldpt*)py]BPh_4	273		4.54	16.6	90	S3
9	[Fe(*saldpt*)py]BPh_4	310		5.42	17.5	150	S3
10	[Fe(*saldpt*)(*atz*)]	416		15.3	36.8	284	S6
11	[Fe(*napet*)(N_3)]	122 ↑, 117 ↓	5	1.53	11.2	99	S4
12	[Fe(*napet*)(NCS)]·MeCN	151		1.92	12.5	87	S4
13	[Fe(*napet*)(NCO)]	155		2.54	16.3	102	S4
14	[Fe(*napet*)(NCSe)]·MeCN	170		2.29	13.3	99	S4
15	[Fe(*napet*)(NCS)]	174		3.08; 0.90	17.1; 5.0	135	S5
16	[Fe(*napet*)(NCS)]·MEK	84					S7
17	[Fe(*napet*)(NCS)]·DMF	235 ↑, 232 ↓	3				S7
18	[Fe(*napet*)(NCS)]·DMSO	138 ↑, 127 ↓	11				S7
19	[Fe(*napet*)(NCSe)]·DMF	244					S7

[a] Abbreviations for petadentate ligands:
H_2(^{3}EtO-*saldet*) = N,N'-bis(3-ethoxy-2-hydroxybenzylidene)-1,5-diamino-3-azapentane),
H_2(^{5}Cl-*salpet*) = N,N'-bis(5-chloro-2-hydroxybenzylidene)-1,6-diamino-3-azahexane),
H_2(^{3,5}Cl-*salpet*) = N,N'-bis(3,5-di-chloro-2-hydroxybenzylidene)-1,6-diamino-3-azahexane),
H_2(*napet*) = *N*,*N*'-bis(2-hydroxynapthylidene)-1,6-diamino-3-azahexane,
H_2(*saldpt*) = *N*,*N*'-bis(2-hydroxybenzyliden)-1,7-diamino-4-azaheptane,
H_2(^{5}Cl-*saldpt*) = *N,N′*-bis(5-chloro-2-hydroxybenzyliden)-1,7-diamino-4-azaheptane,
H_2(^{3}MeO-*saldpt*) = *N,N′*-bis(3-methoxy-2-hydroxybenzyliden)-1,7-diamino-4-azaheptane,
H*atz* = 5-aminotetrazole.

References to Table S3

S1 C. Krüger, P. Augustín, Ľ. Dlháň, J. Pavlik, J. Moncoľ, I. Nemec, R. Boča, F. Renz, *Polyhedron*, 87(2015) 194.
S2 C. Krüger, P. Augustín, I. Nemec, Z. Trávníček, H. Oshio, R. Boča, F. Renz, *Eur. J. Inorg. Chem*. (2013) 902.
S3 R. Boča, Y. Fukuda, M. Gembický, R. Herchel, R. Jaroščiak, W. Linert, F. Renz, J. Yuzurihara, *Chem. Phys. Lett*. 325 (2000) 411.
S4 I. Nemec, R. Herchel, R. Boča, Z. Trávníček, I. Svoboda, H. Fuess. W. Linert, *Dalton Trans*. 40 (2011) 10090.
S5 P. Masárová, P. Zoufalý, J. Moncoľ, I. Nemec, J. Pavlik, M. Gembický, Z. Trávníček, R. Boča, I. Šalitroš, *New. J. Chem*. 39 (2015) 508.
S6 R. Herchel, Z. Trávníček, *Dalton Trans*. 42 (2013) 16279.
S7 I. Nemec, R. Herchel, Z. Trávníček, *Dalton Trans*. 44 (2015) 4474.

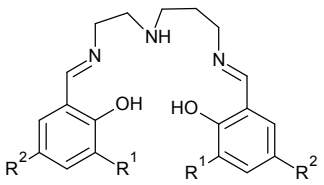

H_2(^{3}R^1,^{5}R^2-*salpet*)

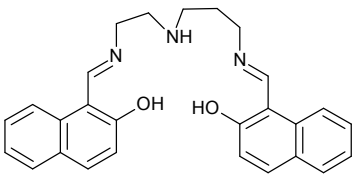

H_2(*napet*)

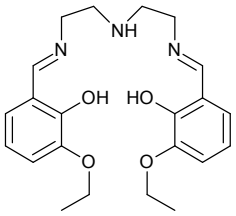

H_2(^{3}EtO-*saldet*)